AUTOMATED K-WISHART CLUSTERING OF POLSAR IMAGES

Anthony P. Doulgeris[1], **Stian N. Anfinsen**[1], **and Torbjørn Eltoft**[1]

[1]*University of Tromsø, The Auroral Observatory, 9037 Tromsø, Norway*
anthony.p.doulgeris@uit.no, stian.normann.anfinsen@uit.no, torbjorn.eltoft@uit.no

ABSTRACT

This paper presents our automatic image segmentation method for Polarimetric SAR data [1] with recent improvements by using matrix log-cumulant methods throughout. The clustering algorithm utilises the full polarimetric matrix information, incorporates texture by modelling with a non-Gaussian distribution, and automatically determines the appropriate number of classes with goodness-of-fit statistical tests. The modelling is based upon the well known product model, with a Gamma distributed texture parameter, leading to the K-Wishart model for the covariance matrix. The automatic clustering is achieved through a modified Expectation Maximisation algorithm, with an additional Goodness-of-fit test allowing splitting and merging of clusters. The resulting image segmentation depicts the statistically significant clusters within the image. Real world examples are shown to demonstrate the technique.

Key words: Polarimetric; Synthetic Aperture Radar; Non-Gaussian; Wishart; Clustering; log-cumulants.

1. INTRODUCTION

Satellite-borne Synthetic Aperture Radar (SAR) systems are well suited to environmental monitoring because of their cloud penetrating ability, day/night operation and broad coverage. Reliable automated image classification schemes are required because of the huge scale of earth monitoring and the wealth of new data scenes available from several new SAR satellite systems.

Pixel-wise analysis of SAR imagery is generally complicated due to the presence of speckle and requires that statistical modelling methods are employed. It is well known that radar speckle is often non-Gaussian in distribution. For this reason, various non-Gaussian models have been proposed to represent SAR data. These have later been extended into the polarimetric realm, where the multivariate K-distributions [2, 3] and G-distributions [4] are successful examples. Both these distributions are members of the so-called product model [5], which states that, under certain conditions, the backscattered signal results from the product between a Gaussian speckle noise component and the textured terrain backscatter. Associated with these models is a so-called non-Gaussianity parameter, which accounts for deviation from Gaussian statistics.

Fully polarimetric SAR (PolSAR) or quadruple polarisation (quad-pol) imagery contains the full scattering matrix information which leads to the best classification results [6]. In addition, full polarimetric SAR images also allow for classification of pixels by dominant scattering mechanisms. Fully polarimetric data is not always available because the wider coverage of dual (dual-pol) or single polarisation modes are often preferred for monitoring purposes.

Polarimetric classifications are commonly performed with the Gaussian based Wishart clustering algorithm. In this study, we use the more advanced non-Gaussian K-Wishart clustering algorithm [7], that additionally accounts for potential textural differences in the classes. This is an Expectation Maximisation (EM) type algorithm, which performs model parameter estimation and Bayesian classification according to an iterative processing scheme. It differs from the standard Wishart because the underlying model for the scattered signal is based on the multivariate K distribution rather than the Gaussian. In addition to the class parameters that are estimated within the EM-based clustering algorithm, we have automated otherwise *a priori* parameters for these statistical models. That is, the effective number of looks (ENL) is automatically determined within the algorithm and is corrected for textural bias, and the appropriate number of classes is determined by a goodness-of-fit test stage within the EM-algorithm that allows for splitting or merging of classes. The result is an automatic image segmentation depicting the statistically distinct classes within the image and subsequent automatic, or assisted, labelling of the found classes may be performed using polarimetric decompositions or any, even limited, ground truth data.

In this paper, we show how non-Gaussianity and polarimetry can be incorporated into practical, automatic and general methods to analyse SAR image data. The methods are generic in the sense that they can be applied to single, dual or quad-pol data, of any frequency, in a common way. Real world examples from Agricultural fields and Arctic glaciers demonstrate the automatic segmentation results of this modelling. These procedures

may become the basis of operational monitoring with SAR systems.

In this paper, section 2 describes the product model and texture, section 3 details the K-Wishart model and section 4 explains the automatic algorithm. Results are shown in section 5, followed by the conclusions.

2. TEXTURE AND THE PRODUCT MODEL

The full complex scattering matrix includes the four combinations of horizontal and vertical polarisation for both the transmitted and received signals. These four channels, HH, HV, VH and VV, together are referred to as quad-pol data, and contain the complete vector information of the scattered signal with respect to the satellite antenna system. These four complex scattering coefficients can be represented as a 4-dimensional complex vector, $\mathbf{s}$, and correspond to the single-look complex (SLC) data format.

Non-Gaussian scattering coefficients have been observed for high resolution and highly textured target regions. Many authors have noted better model fits to class histograms with non-Gaussian models [8, 2, 4], and although there are several specific functional descriptions they are all based upon the "product model". The well known product model (explained in [5]) presumes that the observed variation in SAR backscatter is composed of two independent components, one describing "texture" and another for Gaussian "speckle". For the semi-symmetric, zero-mean case used to describe radar backscatter from natural terrain, the product model may be written as

$$\mathbf{s} = \sqrt{t}\,\mathbf{\Sigma}^{\frac{1}{2}}\mathbf{n}, \tag{1}$$

where the scale parameter t is a strictly positive random variable (scalar), normalised such that its mean $\bar{t} = 1$, $\mathbf{\Sigma}$ is the polarimetric covariance matrix, and $\mathbf{n}$ is a standardised, complex multivariate Gaussian variable with zero mean and identity covariance matrix, i.e. $\mathbf{n} \sim \mathcal{N}^{\mathcal{C}}(\mathbf{0}, \mathbf{I})$. The general interpretation is that the product model describes 'texture' modulated Gaussian speckle. The texture term is introduced here with a square root because the variable t models the variance of the signal rather than its amplitude.

Since the measured scattering coefficients have a mean value of zero, we have to evaluate the 2nd order statistics in the covariance matrix to estimate scattering properties. The statistical modelling must be carried through to the multi-look complex (MLC) covariance matrix. Generally, this is assumed to be equivalent to applying texture directly to the covariance data, and is modelled as

$$\mathbf{C} = t\,\mathbf{W}_{\mathbf{\Sigma}}^{L}/L, \tag{2}$$

where $\mathbf{W}_{\mathbf{\Sigma}}^{L}$ is complex Wishart distributed [9] with L looks and $\mathbf{\Sigma}$ mean covariance matrix.

A constant texture term would describe purely Gaussian vector data and Wishart covariance data and is observed only for very homogeneous and smooth areas in real SAR images.

3. THE K AND K-WISHART DISTRIBUTIONS

The presence of texture increases the variation beyond that for homogenous areas and produces non-Gaussian distributions for the scattering coefficients and non-Gaussian based, or generalised, Wishart models for the covariance matrices [7]. Among the alternative non-Gaussian models, we choose the K-Distribution for the complex scattering coefficients, and the K-Wishart for the covariance matrix, because they appear to be very good models in many situations and they are quite well known. The non-Gaussian flexibility of the K-Wishart model may be seen in Fig. 1. We shall only investigate multi-look MLC data analysis here, since even SLC vector estimation is performed through the covariance matrix.

The K-Wishart probability density function, with L degrees of freedom, shape (non-Gaussianity) parameter α, mean covariance matrix $\mathbf{\Sigma}$, is given by

$$KW(L,\alpha,\mathbf{\Sigma}) = \frac{2|\mathbf{C}|^{L-d}}{I(L,d)\Gamma(\alpha)|\mathbf{\Sigma}|^{L}} (L\alpha)^{\frac{\alpha+Ld}{2}} \left(\mathrm{tr}(\mathbf{\Sigma}^{-1}\mathbf{C})\right)^{\frac{\alpha-Ld}{2}} \times K_{\alpha-Ld}\left(2\sqrt{L\alpha\,\mathrm{tr}(\mathbf{\Sigma}^{-1}\mathbf{C})}\right) \tag{3}$$

where $\mathrm{tr}(\cdot)$ denotes the trace operation, $|\cdot|$ the determinant, $\Gamma(\cdot)$ as the standard Gamma function, d is the vector dimension, $K_m(x)$ is a modified Bessel function of the second kind with order m and

$$I(L,d) = \pi^{\frac{d(d-1)}{2}} \prod_{i=1}^{d} \Gamma(L-i+1) \tag{4}$$

is a normalisation constant.

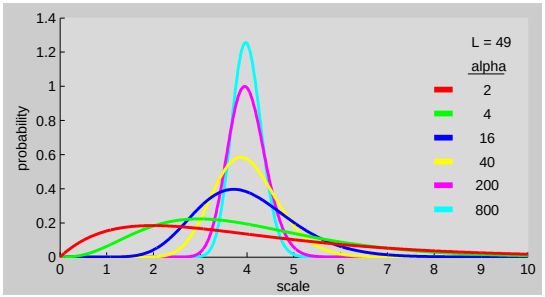

Figure 1. Non-Gaussian flexibility of K-Wishart model with different shape parameter values. 1-D compacted representation of matrix scale with tr$(\mathbf{\Sigma}^{-1}\mathbf{C})$.

All texture parameter estimation is performed with the latest methods of matrix log-cumulants, because log-cumulant based methods are shown to have lower bias and variance compared to other parameter estimators, and are outlined in [10].

The matrix log-cumulants for the K-Wishart model are:

$$\kappa_1\{\mathbf{C}\} = \ln|\mathbf{\Sigma}| + \psi_d^{(0)}(L) - d\ln(L) + d\psi^{(0)}(\alpha) - d\ln(\alpha) \quad (5)$$

$$\kappa_\nu\{\mathbf{C}\} = \quad \psi_d^{\nu-1}(L) + d^\nu\psi^{\nu-1}(\alpha) \quad , \ \nu \geq 2 \quad (6)$$

The goodness-of-fit testing is performed with the new method of matrix log-cumulant goodness-of-fit test statistic described in [11]. For class sample sizes, n, larger then 300, the Chi-squared approximation is used, and for smaller sample sizes the Monte-Carlo simulation method is used, both are described in [11]. This threshold was determined empirically as a compromise between accuracy and speed.

The method of matrix log-cumulant goodness-of-fit test statistic is given by:

$$Q_p \quad = \quad n(\langle\boldsymbol{\kappa}\rangle - \boldsymbol{\kappa})^T\mathbf{K}^{-1}(\langle\boldsymbol{\kappa}\rangle - \boldsymbol{\kappa}) \quad (7)$$

$$Q_p \quad \sim \quad \chi^2(p) \quad (8)$$

where the vector $\langle\boldsymbol{\kappa}\rangle$ is constructed from p sample matrix log-cumulants. Its mean vector $\boldsymbol{\kappa} = E\{\langle\boldsymbol{\kappa}\rangle\}$ and covariance matrix $\mathbf{K} = Cov\{\langle\boldsymbol{\kappa}\rangle\}$ is built up of population matrix log-cumulants of orders up to two times the maximum order contained in $\langle\boldsymbol{\kappa}\rangle$ [11]. That is, for the first four log-cumulants,

$$\mathbf{K} = \begin{bmatrix} \kappa_2 & \kappa_3 & \kappa_4 & \kappa_5 \\ \kappa_3 & \kappa_4 + 2\kappa_2^2 & \kappa_5 + 6\kappa_2\kappa_3 & K_{24} \\ \kappa_4 & \kappa_5 + 6\kappa_2\kappa_3 & K_{33} & K_{34} \\ \kappa_5 & K_{42} & K_{43} & K_{44} \end{bmatrix} \quad (9)$$

where

$$K_{24} = K_{42} = \kappa_6 + 8\kappa_2\kappa_4 + 6\kappa_3^2\,, \quad (10)$$

$$K_{33} = \kappa_6 + 9\kappa_2\kappa_4 + 9\kappa_3^2 + 6\kappa_2^3\,, \quad (11)$$

$$K_{34} = K_{43} = \kappa_7 + 12\kappa_2\kappa_5 + 30\kappa_3\kappa_4 + 36\kappa_2^2\kappa_3\,, \quad (12)$$

$$K_{44} = \kappa_8 + 16\kappa_2\kappa_6 + 48\kappa_3\kappa_5 + 34\kappa_4^2 + 72\kappa_2^2\kappa_4 + 144\kappa_2\kappa_3^2 + 24\kappa_2^4\,. \quad (13)$$

Sample log-cumulants are derived from sample log-moments via the following relations

$$\kappa_1 = \mu_1\,, \quad (14)$$

$$\kappa_2 = \mu_2 - \mu_1^2\,, \quad (15)$$

$$\kappa_3 = \mu_3 - 3\mu_1\mu_2 + 2\mu_1^3\,, \quad (16)$$

$$\kappa_4 = \mu_4 - 4\mu_1\mu_3 - 3\mu_2^2 + 12\mu_1^2\mu_2 - 6\mu_1^4\,, \quad (17)$$

where the sample log-moments, μ_ν, are themselves derived as class weighted means of $(\log|\mathbf{C}_i|)^\nu$.

4. AUTOMATED ANALYSIS

The unsupervised clustering algorithm is based upon the standard expectation maximisation (EM) algorithm [12] for finite mixture modelling, using the K-Wishart expression (3) for the probabilities. The statistical finite mixture model for the whole data-set may be expressed as:

$$f_{\mathbf{C}}(\mathbf{C}) = \sum_{j=1}^{m} \pi_j f_j(\mathbf{C}) \quad (18)$$

where π_j are the class *priors* such that $\sum_{j=1}^{m}\pi_j = 1$ and the $f_j(\mathbf{C})$ are the individual class model PDFs from eqn. (3).

The EM algorithm starts from some initialisation state and iteratively improve the clustering until some convergence criterion is met. The K-Wishart class parameter updates involve membership weighted sums over the covariance matrix data points for the class covariance matrix $\mathbf{\Sigma}$, and weighted matrix log-cumulants for the shape parameter.

The K-Wishart expression (3) requires the number of looks parameter L, which is assumed to be independent looks. In reality, there is some correlation between image data pixels and the number of (correlated) looks needs to be substituted for the effective number of (independent) looks (ENL) to fit the data. The ENL value may be known from the satellite system and the degree of multi-look smoothing applied to the image, or estimated from the data. We estimate the ENL, including a correction for textural bias, directly within the EM-algorithm parameter estimation stage using matrix log-cumulants [10].

A major problem with mixture models in general is that of choosing the appropriate number of mixture classes. In this study, we include a goodness-of-fit stage within the algorithm, that regularly checks the current class estimates versus the models. This allows for a splitting option for clearly mixed, multi-modal clusters, and for a merging of two virtually identical competing clusters. The goodness-of-fit testing is performed using the methods of matrix log-cumulants described in [11] by using the first four log-cumulants. It operates directly on the covariance matrix samples and takes only a statistical confidence level as a sensitivity criterion.

The goodness-of-fit criterion and the number of samples in each class therefore determines how many classes are deemed statistically significant within the image. This also means that the clustering needs no special initialisation, because it can be initialised as one single class and will automatically split and adapt until it is a sufficiently good fit to the data mixture model.

A visual display of the class goodness-of-fit is obtained by plotting the mean squared Mahalanobis measure, $M = \text{trace}(\mathbf{\Sigma}^{-1}\mathbf{C})$, as histograms for each class. This is appropriate because the assumed product model is a scalar product and M averages each dimension of the decorrelated data to produce an effective compaction from a matrix to a one dimensional description, and readily shows the underlying texture variation as increased width and skewness. The parametric model is easily transformed and displayed against the data histograms, since

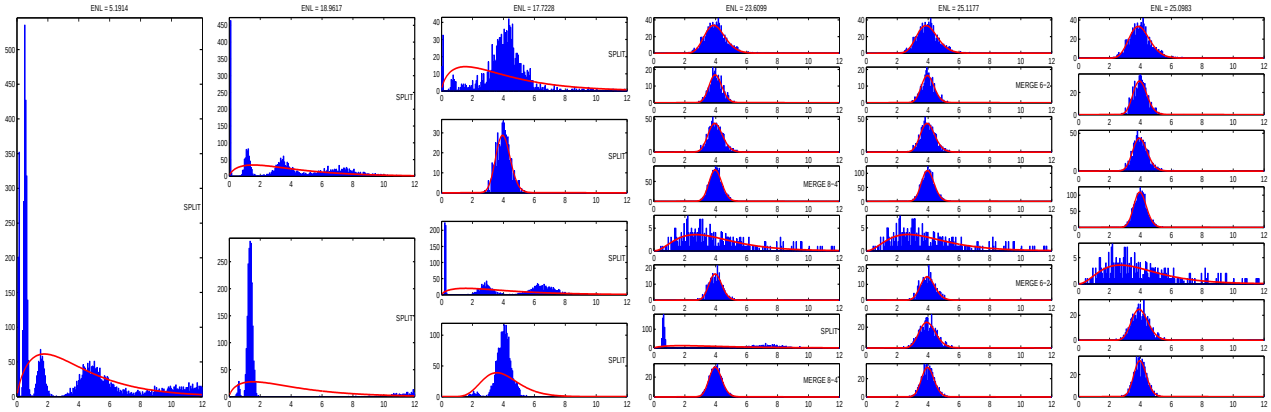

Figure 2. Class histogram sequence (from left to right) of automatic segmentation of 7 class test pattern. Note the poorly fitted classes are split up to 8 classes before merging some identical classes back to the correct 7, well fitting, classes.

the K model is infinitely divisible [13], and the trace sum has $L \times d$ whitened terms and a mean of d. The model curves to compare to the data histograms of M are therefore $KW(Ld, \alpha, d)$ for each of the K-Wishart clusters. We refer to these plots as class histograms. The scale is normalised for each class so inter-comparison is not possible, but the goodness-of-fit of each class is readily apparent.

A sequence of such class histograms are shown in Fig. 2, which depicts the automatic split & merge capability for a test pattern of 7 classes. Note that the number of classes increases to 8 before merging back to 7. The early classes are clearly mixtures of several real clusters of data and are split appropriately. The broadest final histogram (number 5) depicts the most non-Gaussian class.

5. RESULTS: REAL WORLD EXAMPLES

The automatic segmentation will be demonstrated on two small and reasonably simple images such that a visual validation is possible. The first is an agricultural area from an airborne EMISAR, L-band, quad-pol SAR flight over Foulum Denmark in 1998 (also analysed and described in [7]), and the other is from an Envisat, C-band, dual-Pol ASAR image over Kongsvegen glacier, Svalbard in 2005 (previously analysed in [6]).

Fig. 3 shows an enhanced Pauli RGB image (top) and the subsequent "coarse" segmentation (sub-sampling to 1/36 of the data size), which automatically found 6 distinct classes. Visual comparison with the Pauli image confirms that the major fields are cleanly segmented and distinguished, and that the different classes within the forest (the large whitish areas in the Pauli) clearly match the brighter/darker regions within the forest. Overall this gives a visually satisfactory segmentation.

Four times as many samples results in 12 classes (shown if Fig. 4), with more small classes being supported, for example around the borders of fields and near the buildings, yet retains the nice "solid" field segments as before.

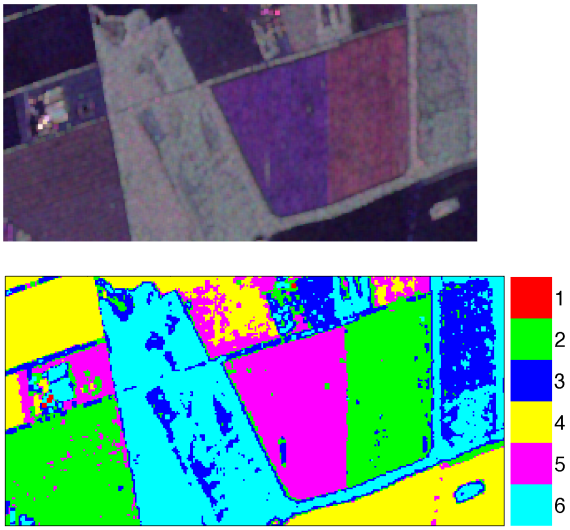

Figure 3. Pauli RGB image (top) and Auto-Segmentation of Foulum dataset, 18 looks, low sample size, 6 classes.

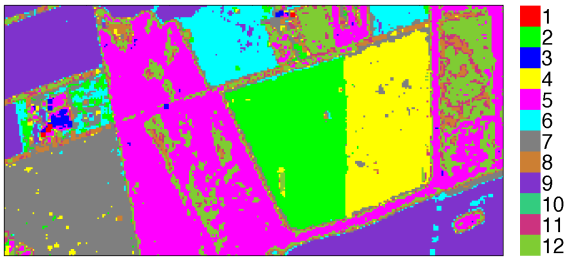

Figure 4. Auto-Segmentation of Foulum dataset, 18 looks, larger sample size, 12 classes.

Fig. 5 shows the results of a "coarse" (1/100 sub-sampling) segmentation of the dual-pol glacier data. The mountains have been masked out for convenience, and again a careful comparison with the Pauli image (top) in-

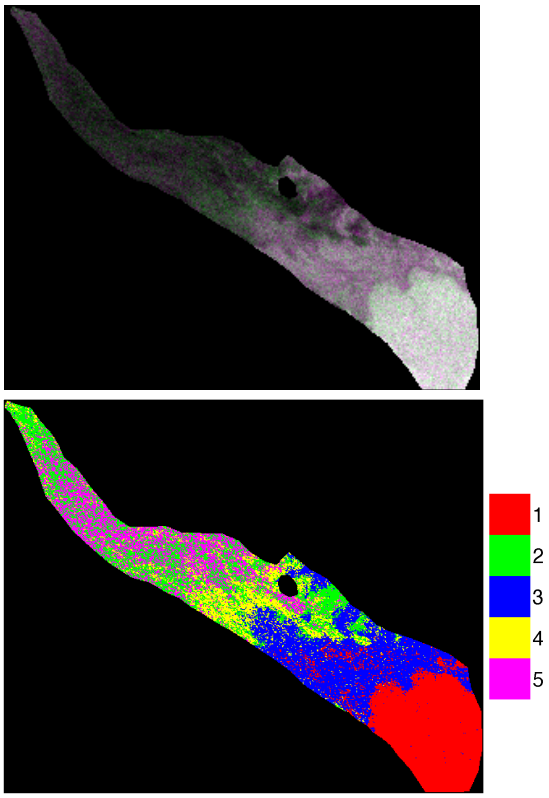

Figure 5. Pauli RGB image (top) and Auto-Segmentation of Kongsvegen dataset, 40 looks, low sample size, 6 classes.

dicates that it has successfully found the major brightness and polarimetric classes within the image. Less sub-sampling would result in more smaller classes as expected, but becomes more complicated visually.

6. CONCLUSIONS

We have demonstrated an operational automatic segmentation method that incorporates both polarimetry and non-Gaussian analysis with good results. The dependence on sample sizes to statistically support the number of classes is expected and desirable, since it gives the opportunity to do either "fine" or "coarse" analyses and potentially save processing time. The goodness-of-fit tests can be readily visualised with the class histograms and seems appropriate through visual inspection.

The split and merge options through goodness-of-fit testing at the class level can be applied to other situations and mixture models too, and only requires that the class probability density functions and log-cumulant expressions are known. The use of log-cumulants throughout the algorithm has simplified the goodness-of-fit testing as it now operates directly upon the matrix-variate data pixels at the chosen statistical confidence level. The method is generalised to any number of polarimetric channels, and was demonstrated on both quad-pol L-band and dual-pol C-band scenes.

REFERENCES

[1] Anthony P Doulgeris and Torbjørn Eltoft. Automated Non-Gaussian clustering of polarimetric SAR. In *8th European Conference on Synthetic Aperture Radar (EUSAR2010)*, Aachen, Germany, June 7-10 2010.

[2] J. S. Lee, D. L. Schuler, R. H. Lang, and K. J. Ranson. K-distribution for multi-look processed polarimetric sar imagery. In *IEEE Int. Geosci. Remote Sensing Symp.*, pages 2179–2181, 1994.

[3] A. Doulgeris and T. Eltoft. Scale mixture of Gaussians modelling of polarimetric SAR data. In *International POLinSAR Workshop (POLinSAR2007)*, Frascati, Italy, January 22-26 2007.

[4] Corina C. Freitas, Alejandro C. Frery, and Antonio H. Correia. The polarimetric G distribution for SAR data analysis. *Environmetrics*, 16:13–31, 2005.

[5] C. Oliver and S. Quegan. *Understanding Synthetic Aperture Radar Images*. SciTech Publishing, Raleigh, USA, 2nd edition, 2004.

[6] A.P. Doulgeris, S.N. Anfinsen, Y. Larsen, K. Langley, and T. Eltoft. Evaluation of polarimetric configurations for glacier classification. In *International POLinSAR Workshop (POLinSAR2009)*, Frascati, Italy, January 26-30 2009.

[7] A.P. Doulgeris, S.N. Anfinsen, and T. Eltoft. Classification with a non-gaussian model for polsar data. *IEEE Trans. Geoscience and Remote Sensing*, 46(10):2999–3009, Oct. 2008.

[8] E. Jakeman and P. N. Pusey. A model for non-Rayleigh sea echo. *IEEE Trans. Antennas Propagat.*, 24, 6:806–814, November 1976.

[9] J.S. Lee, M.R. Grunes, and R. Kwok. Classification of multi-look polarimetric SAR imagery based on the complex Wishart distribution. In *Int. J. Remote Sensing*, volume 15, 11 1994.

[10] Stian Normann Anfinsen and Torbjørn Eltoft. Application of the Matrix-Variate Mellin Tranform to Analysis of Polarimetric Radar Images. *IEEE Trans. Geoscience and Remote Sensing*, 49(7):15 pp., in press, July 2011.

[11] Stian Normann Anfinsen, Anthony P Doulgeris, and Torbjørn Eltoft. Goodness-of-Fit Tests for Multilook Polarimetric Radar Data Based on the Mellin Transform. *IEEE Trans. Geoscience and Remote Sensing*, 49(8):18 pp., in press, August 2011.

[12] A. P. Dempster, N. M. Laird, and D. B. Rubin. Maximum likelihood from incomplete data via the EM algorithm. *Journal of the Royal Statistical Society. Series B*, 39(1):1–38, 1977.

[13] E. Jakeman and R. J. A. Tough. Generalized K distribution: a statistical model for weak scattering. *J. Opt. Soc. Am. A*, 4, 9:1764–1772, September 1987.